APPLICATIONS OF
MODELLING AND SIMULATION
http://arqiipubl.com/ams eISSN 2600-8084 VOL 8, 2024, 121-131

Numerical Analysis on the Hemodynamic Effects of Asymmetric Stenosis at High Heart Rate in the Left Coronary Artery Bifurcation

Asif Equbal* and Paragmoni Kalita

Department of Mechanical Engineering, Tezpur University, Assam-784028, India

*Corresponding author: asifraj321@gmail.com

Submitted 29 January 2024, Revised 08 April 2024, Accepted 20 April 2024, Available online 16 May 2024.
Copyright © 2024 The Authors.

Abstract: The branches of the left coronary artery are more critical compared with the right counterpart from the perspective of atherosclerosis and associated heart diseases. Most of the preceding research works studied axisymmetric stenosis shapes in coronary artery bifurcation. However, recent studies indicate that coronary artery blockages are often asymmetric in structures. The present work carries out a novel numerical investigation on the effects of asymmetric degree of stenosis (DOS) having the more typical cosine shape by considering the branches of the left coronary main (LCM) artery, namely, the left circumflex (LCx) and left anterior descending (LAD). The results are analysed to correlate the influence of stenosis in LCx and LAD to the disease severity and progression in terms of hemodynamic parameters including wall shear stress (WSS) profiles, oscillatory shear index (OSI), and pressure drop (PD). The computations reveal that WSS attains lower values over wider regions in the post-stenotic regions in LAD compared with LCx. The values of OSI in the LAD are also higher compared to LCx in all the cases. The peak value of the OSI decreases with the increase in the DOS. However, for higher stenosis degrees, the prominence of OSI is observed even at larger distances in the post-stenosis region. At a given DOS, PD is more in LAD compared with LCx. These effects are found to increase with DOS.

Keywords: Atherosclerosis; Computational fluid dynamics; Coronary artery; Hemodynamics; Stenosis.

1. INTRODUCTION

In recent years cardiovascular disorders have emerged as the leading cause of death worldwide. About 17.9 million individuals died from cardiovascular disorders in 2019, with heart attacks and strokes accounting for 85% of these occurrences [1]. The coronary artery is the blood vessel that supplies sufficient quantity of oxygenated blood to the heart for its proper functioning. The accumulation of plaque in the coronary artery narrows the cross-sectional area of the blood vessel, which in turn lowers cardiac blood flow. The accumulation of atherosclerotic plaque may cause heart dysfunction and death [2,3]. The development of medical imaging technology has been extensively used in recent decades to diagnose atherosclerosis. However, other than for phase contrast, it could not give comprehensive hemodynamic information for arterial abnormalities. Computational modelling in conjunction with medical imaging could offer a promising alternative for addressing these kinds of problems [4]. Therefore, computational fluid dynamics (CFD) can be a very useful tool for the analysis and prediction of disease progression due to atherosclerosis.

Several research findings indicate that the structure and function of coronary arteries can exhibit considerable variation as a result of hemodynamic forces. The constant contact of the endothelium layer and the luminal surface with blood flow gives rise to hemodynamic shear forces. Stenosis initiates and progresses when these hemodynamic forces are insufficient to maintain the physiological threshold [5]. Chaichana *et al.* [6] postulated that in terms of atherosclerosis and heart diseases, the left coronary main (LCM) and its branches were more crucial than their counterparts on the right side. Various studies have been reported to link atherosusceptibility in coronary artery trees with different hemodynamic parameters [7–9].

Several studies have been reported in the literature on the hemodynamics through standalone arteries with axisymmetric or asymmetric stenosis. Ang and Mazumdar [10] studied mathematical simulations of blood flow via an artery with asymmetric stenosis. Frattolin *et al.* [11] numerically investigated the effects of axisymmetric stenosis severity and locations on the flow distribution and WSS of the LCM, LCx and LAD branches. Kamangar *et al.* [12] investigated the influence of axisymmetric stenosis on the hemodynamics of patient-specific left coronary arteries. Song *et al.* [13] performed a CFD analysis of a transient model of coronary artery bifurcation with axisymmetric stenosis of various severities, lengths, and heart rates. Tian *et al.* [14] performed a numerical simulation for a two-dimensional (2D) straight artery with asymmetric stenosis on the lower

This article is distributed under a Creative Commons Attribution 4.0 License that permits any use, reproduction and distribution of the work without further permission provided that the original work is properly cited.

wall for both steady and pulsatile inlet velocity conditions by using the Carreau Yasuda model. Sood *et al.* [15] studied the effects of heart rate (HR) on the space- and time-dependent variations of WSS and OSI by considering axisymmetric as well as asymmetric forms of stenosis on straight arteries. Thomas *et al.* [16] presented a patient-specific study of hemodynamics in a Coronary Artery with asymmetric stenosis. Timofeeva *et al.* [17] carried out a CFD study on the effects of different degrees of asymmetric stenosis and eccentricity on the hemodynamics of a stand-alone LAD artery.

Many studies have investigated the impact of hemodynamic parameters on atherosusceptibility in coronary artery bifurcations, primarily focusing on axisymmetric stenosis. However, research on asymmetric stenosis has largely been limited to individual arteries, neglecting comprehensive analyses. Notably absent from the literature are numerical studies investigating the hemodynamic impacts of varying degrees of asymmetric stenosis in artery-tree models encompassing the LCM and its primary branches. Specifically, there is a lack of comparative analyses regarding the effects of varying degrees of asymmetric stenosis in LCx and LAD arteries. Additionally, recent attention from researchers has been drawn to sudden cardiac arrests and fatalities occurring during strenuous physical activity among individuals with known or undiagnosed cardiovascular conditions [18–20]. A HR of 120 beats per minute (bpm) signifies high-intensity exercise conditions. Particularly, the flow rate per cycle was held constant across heart rates of 75, 100, and 120 bpm [13]. At 120 bpm, the maximum velocity within the cycle is highest due to the shortest cycle time, leading to the highest peak WSS. Additionally, peak OSI values are elevated due to vortex shedding in the post-stenotic region [21]. The present study's primary contribution lies in providing a direct relative assessment of the severity of disease resulting from asymmetric stenosis in LAD and LCx arteries under high HR conditions. It may be noted that the bifurcation zones facing the flow separators are susceptible to atherosclerosis progression [22–24]. Hence, this study employs numerical analysis to examine pulsatile blood flow through the left coronary artery tree by considering different degrees of asymmetric stenosis in the LCx and LAD branches at a heart rate of 120 bpm. Extensive numerical investigations are carried out to analyse the effects of degree of stenosis (DOS) on the potential disease progression by correlating with the important hemodynamic parameters including WSS, OSI, and PD.

This paper is organised into five sections. The methodology, including the numerical methods and validation of the methodology, are explained in Section 2. The hemodynamic parameters analysed in the current study are presented in Section 3 before presenting the results and discussion in Section 4. Concluding remarks are made in Section 5.

2. METHODOLOGY

2.1 The Geometrical Modelling of the Present Study

A 2D model of the left coronary artery and its branches is constructed from data available in the literature [25,26]. The relevant geometrical details of the artery and its branches including the different vessel diameters, lengths and the angles are presented in Figure 1(a). The stenotic constrictions may take any geometrical shape [27]. However, in our study, the more typical and realistic cosine-shaped stenosis is considered for the LCx and LAD branches [28,29]. The starting location of stenosis is considered at 1.5 mm from the bifurcation point [13]. Medical observations suggest that the length of the plaque in the coronary artery varies from 1 to 3 times the vessel diameter [30]. Accordingly, the length of stenosis is taken as 6.28 mm. Here four different degrees of stenosis, viz., 30%, 45%, 60%, and 75% are considered for both vessels under the study. These are represented in Figure 1(b) and Figure 1(c). The % DOS is evaluated based on the ratio of diameter at the stenosis and normal regions [31] as given in Equation (1).

$$\mathrm{DOS} = \left(1 - \frac{D_{\mathrm{blockage}}}{D_{\mathrm{normal}}}\right) \times 100 \tag{1}$$

where D_{blockage} and D_{normal} are the diameters of the artery at the stenosis and normal regions, respectively. From Figure 1(a) it can be worked out that the stenosis centres are located at $\mathrm{X}' = \mathrm{X}'' = 4.64$ mm both in LCx and LAD.

2.2 Governing Equations

Mathematical modelling of blood flow is quite challenging because blood changes its viscosity with the shear rate, the arteries are not rigid, and the flows are pulsatile and potentially turbulent in some cases. Accounting for all the complexities of blood flow makes the analysis highly complicated. Accordingly, some reasonable simplifications in the modelling are called for. The peak Reynolds number, resulting from pulsatile blood flow, occurs at the largest vessel diameter under maximum flow conditions during each pulse cycle. This is determined as follows:

$$\mathrm{Re} = \frac{\rho D v}{\mu} = \frac{1060 \times 4.5 \times 10^{-3} \times 0.345}{0.00345} = 477 \tag{2}$$

where, ρ, D, v, and μ are the blood density, diameter of the left coronary main artery, the maximum velocity during the pulse cycle and high-shear-rate dynamic viscosity of the blood respectively. Therefore, we rationalise the model by considering the flow to be laminar. Additionally, the blood flow is modelled as homogenous, incompressible, and non-Newtonian with negligible body force [5,28,32]. Under these assumptions, the continuity and momentum equations governing the blood flow through the artery can be represented as follows:

$$\nabla . \mathbf{U} = 0 \tag{3}$$

$$\frac{\partial(\rho \mathbf{U})}{\partial t} + \nabla . (\rho \mathbf{U}\mathbf{U}) = -\nabla p + \nabla . \boldsymbol{\tau} \tag{4}$$

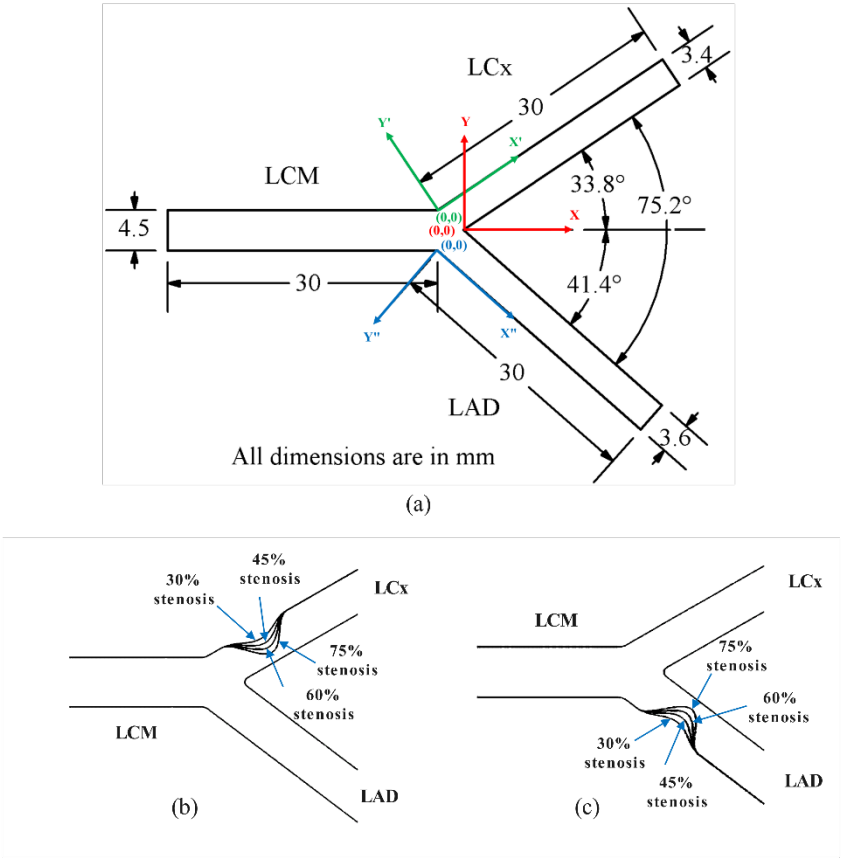

Figure 1. 2D model of left coronary artery and its branches: (a) Without stenosis, (b) With stenosis in LCx vessel, (c) With stenosis in LAD vessel.

where **U** is the velocity vector, ρ is the density of blood with a value of 1060 kg/m^3 [27,32], p is the pressure and $\boldsymbol{\tau}$ is the viscous stress tensor. The Carreau viscosity model is used in our study due to its high accuracy in the computation of blood flows through arteries as suggested by [33]. The corresponding constitutive equation is written as [34]

$$\mu = \mu_\infty + (\mu_0 - \mu_\infty)[1 + (\lambda\dot{\gamma})^2]^{\frac{n-1}{2}} \tag{5}$$

where μ is the blood viscosity, $\dot{\gamma}$ is the local shear rate, λ is relaxation time, n is the power index, and μ_0 and μ_∞ are the viscosity at zero and high shear rates, respectively. The values of all four coefficients for human blood are taken from [33]. The relationship between stress tensor ($\boldsymbol{\tau}$), viscosity (μ), and shear rate tensor (**D**) is given by [34]

$$\boldsymbol{\tau} = 2\mu(\dot{\gamma})\mathbf{D} \tag{6}$$

where $\mathbf{D} = \begin{bmatrix} \frac{\partial u}{\partial x} & \frac{1}{2}\left(\frac{\partial u}{\partial y} + \frac{\partial v}{\partial x}\right) \\ \frac{1}{2}\left(\frac{\partial u}{\partial y} + \frac{\partial v}{\partial x}\right) & \frac{\partial v}{\partial y} \end{bmatrix}$.

2.3 Boundary Conditions

Several research works in the past decades considered the steady-state model for blood flow in the arteries. However, pulsatile blood flow is considered a more realistic model for hemodynamics study [35]. Thus, in the present work, the pulsatile boundary conditions for exercise conditions are applied at the inlet and outlet. Here the waveforms for 120 bpm are taken from [13]. The velocity form thus obtained applied as velocity inlet boundary condition is shown in Figure 2(a). The pressure outlet boundary condition is applied with the corresponding pulsatile pressure variation, as shown in Figure 2(b). The arterial wall is considered to be rigid, and the no-slip condition is applied to it. This is a reasonable assumption because coronary artery problems generally develop with ageing as the artery walls become stiffer and tougher [27].

2.4 The Numerical Schemes, Grid and Time Step Independence Studies

The commercial finite volume CFD package ANSYS Fluent (ANSYS® Academic Research [Fluent], release 14) is employed in the present investigation. The flow domain is discretized with a quadrilateral grid using the face-meshing technique built into the ANSYS meshing tool. The meshes in the bifurcation zone and stenosis region are refined to capture flow physics accurately as shown in Figure 3. The convective terms in the momentum equation are computed using a second-order upwind technique, whereas the pressure is calculated using a second-order discretization. The Semi-Implicit approach for Pressure-

linked Equations (SIMPLE) approach is used to couple pressure and velocity fields. The maximum time iteration per time step is assigned as 10 and the residuals of all variables are set to10^{-5} for the convergence of the results. Figure 4(a) plots the velocity profiles on a cross section at an axial location of $2 \times D$ after the post-stenosis region in LCx for different grid sizes with 60% DOS. Four different grid sizes with 4971, 9528, 17335, and 32637 cells are tested. The mesh independence is attained with the grid having 17335 cells. The same grid is now considered for the time step independence study. Four different time steps (0.01, 0.005, 0.001, 0.0005) are used to check the unsteady simulations, which are shown in Figure 4(b). It shows that the time-step independence is attained for the time step of 0.001.

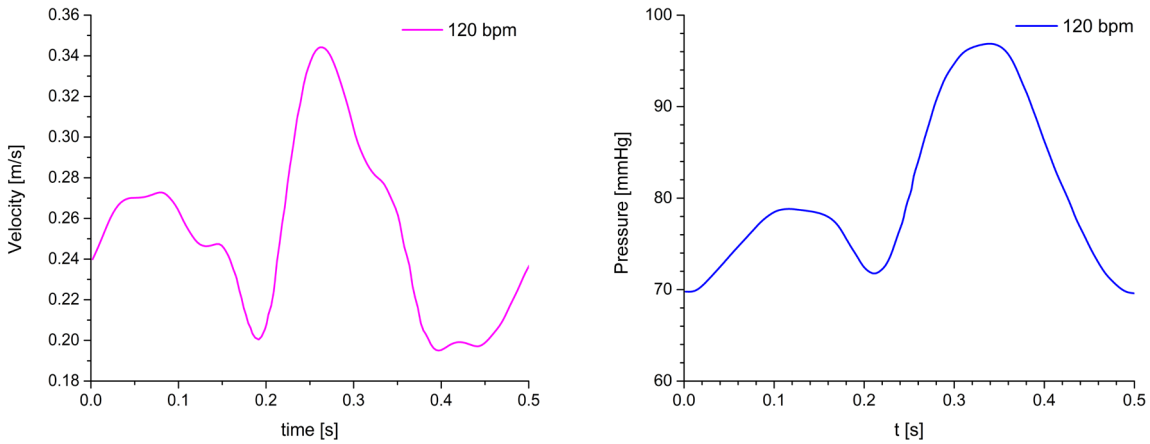

Figure 2. Pulsatile waveform for 120 bpm: (a) Velocity inlet, (b) Corresponding pressure outlet.

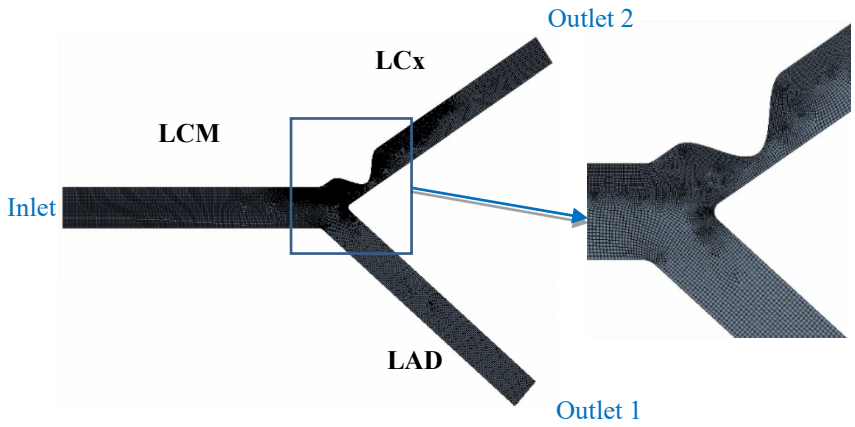

Figure 3. Mesh of the artery model.

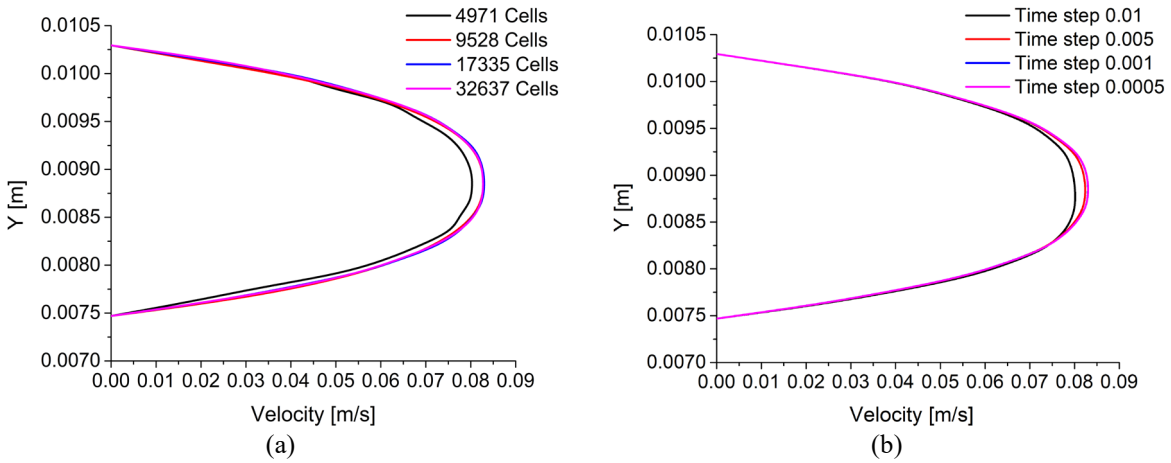

Figure 4. LCx vessel with 60% stenosis: (a) Grid-independence study, (b) Time-step independence study.

2.5 Validation of the Numerical Model

The validation study consists of steady blood flow through a straight artery with asymmetric stenosis [28]. The simulations are carried out using the numerical schemes stated in Section 2.4. Figure 5(a) and Figure 5(b) compare the wall shear stress and wall pressure variations, respectively, of our work with the results of [28]. The results of the present numerical simulation are found in excellent agreement with the reference results.

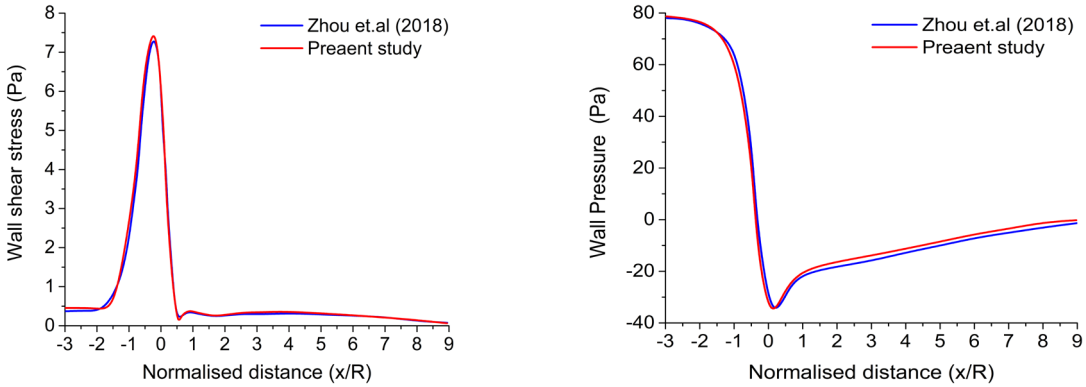

Figure 5. Validation of the present model with Zhou *et al.*'s work for 75% degree of stenosis: (a) Wall shear stress variation, (b) Wall pressure variation.

3. HEMODYNAMIC PARAMETER OF THE STUDY

To understand the pathological issues and their diagnosis for stenosed arteries we must deal with the factors which severely affect the dynamics of blood flow. The important hemodynamic parameters relevant to the health of vascular tissues are discussed here.

3.1 Wall Shear Stress

Wall shear stress (WSS) is the tangential force of the blood acting per unit area on the wall of the vessel due to the flow. It is calculated as the product of viscosity and velocity gradient at the wall [36,37] shown in Equation (7).

$$\text{WSS} = \mu \left(\frac{\partial u_t}{\partial \eta}\right)_{\eta=0} \tag{7}$$

where u_t is velocity component tangential to the arterial wall, η is the distance normal to the wall, and μ is the dynamic viscosity of the fluid at the vessel wall. Regions with WSS less than 1 Pa are considered to be athero-prone sites as the endothelial function is significantly affected in such areas [22,38].

3.2 Oscillatory Shear Index

It is a dimensionless hemodynamic parameter developed by [39], which is calculated based on the ratio of time-averaged magnitude of the WSS vector and the time-averaged wall shear stress vector (TAWSS). It signifies the alignment of the WSS vector with the TAWSS during the cardiac cycle [40]. In other words, OSI signifies the cyclic deviation of the wall shear stress vector from its predominant axial orientation, The OSI is determined by Equation (8).

$$\text{OSI} = \frac{1}{2}\left[1 - \frac{\tau_{mag}}{\tau_{\text{mean}}}\right] \tag{8}$$

where τ_{mean} or TAWSS and τ_{mag} are presented in Equations (9) and (10), respectively.

$$\tau_{mean} = \text{TAWSS} = \frac{1}{T}\int_0^T |\boldsymbol{\tau}_w|\, dt \tag{9}$$

$$\tau_{mag} = \left|\frac{1}{T}\int_0^T |\boldsymbol{\tau}_w dt|\right| \tag{10}$$

Here $|\boldsymbol{\tau}_w|$ is the magnitude of instantaneous WSS in N/m^2 and T is the pulse period in seconds. The value of OSI lies between 0 to 0.5. A value of 0 indicates that the WSS vector has no cyclic deviation, whereas a value of 0.5 indicates that the WSS vector has a 180° deviation or purely oscillatory flow. A high value of OSI particularly greater than 0.3 creates a favourable environment for the development of atherosclerosis [23].

3.3 Pressure Drop

Pressure Drop (PD) is a crucial metric in the hemodynamic study of a coronary artery system**.** The pressure inside the artery drops significantly because of plaque formation. The pressure drop across the plaque helps to identify the severity of the stenosis [41]. The widely-used clinical parameter fractional flow reverse (FFR) also works based on the pressure drop principle [22]. It is calculated by Equation (11).

$$\mathrm{PD} = p_{\mathrm{bp}} - p_{\mathrm{ep}} \tag{11}$$

where p_{bp} is the pressure at the beginning point of the stenosis and p_{ep} is the pressure at the endpoint of the stenosis.

4. RESULTS AND DISCUSSION

The simulations are performed for three cardiac cycles to minimize the cyclic inaccuracies in the results. Accordingly, in the present work, all the results on spatial variations of the hemodynamic parameters are presented at the end of the third cycle as suggested in the references [32,42]. The computer used for the present simulations has a configuration of 4 cores and 8 threads with a base clock speed of 3.19 GHz. Figure 6 represents five stages of the heart cycle, namely, end-systole, early diastole, peak diastole, end-diastole, and early systole on a plot of average velocity at inlet vs time for a heart rate of 120 bpm.

Figures 7(a)-(e) plot the $x-$ velocity streamlines of the LCx and LAD vessels at different instants of the heart cycle for 75% of stenosis in each branch. A close inspection of the plots reveals that recirculation zones are generated on the upstream and downstream ends of the plaque with negative velocities in both branches at all stages. In both the vessels negative velocities appear for all DOS. The minimum velocities in LAD are lower than corresponding values LCx in all cases. The lowest velocities of -0.135 m/s and -0.139 m/s are attained just downstream of the stenosis at the peak diastole stage for LCx and LAD, respectively. These recirculation zones with negative velocities are highly athero-prone sites as negative wall shear stresses are developed in such regions. On the other hand, the maximum velocities of 0.452 m/s and 0.449 m/s are observed at peak diastole both in the case of LCx and LAD, respectively. At this stage, large circulation zones with vortex shedding are observed in the post-stenosis regions in both branches. This can be attributed to a jet of high velocity experiencing a sudden enlargement of the flow area. The vortex shedding results in the formation of alternating low-pressure zones downstream of the stenosis, which results in wavering forces on the fluid body. This in turn will lead to time oscillation of the WSS, further having the potential to cause elevated levels of OSI. Smaller recirculation zones are created for higher velocities at other time instants of the pulse as well. A similar observation was noted by [15] in the case of a straight artery.

Figure 8 displays the WSS variations at the different degrees of stenosis in the LCx and LAD vessels. It demonstrates that WSS approaches its peak just downstream of the stenosis centre. The peak value of WSS increases with the increase in degree of stenosis both in the cases of LCx and LAD. In LCx, the maximum computed WSS is 10.42 Pa at 75% DOS at 6.14 mm from the bifurcation point along the vessel, i.e., at $\mathrm{X}' = 6.14$ mm (Figure 1(a)). On the other hand, the maximum value of WSS attained in LAD is 11.56 Pa at the same DOS and HR at 6.84 mm from the bifurcation point, i.e., at $\mathrm{X}'' = 6.84$ mm (Figure 1(a)). However, sharp drops in WSS are observed just on the upstream and downstream sides of the peak-WSS location, owing to disturbances to flow caused by the flow constriction. Our study shows that negative WSS is reached at all degrees of stenosis in LCx and LAD. At all degrees of stenosis, the lowest values of WSS in LAD are lower than the corresponding ones in LCx. The minimum value of WSS registered in the LCx and LAD are -0.49 Pa and -0.67 Pa downstream of the plaque at 75% DOS. These zones of negative WSS are caused by the strong recirculation zones created in the flow field due to the flow obstruction. It can be inferred from the analysis of WSS profiles that LAD is more prone to faster disease progression than LCx for all DOS, owing to lower values of WSS attained in wider areas of the post-stenotic region.

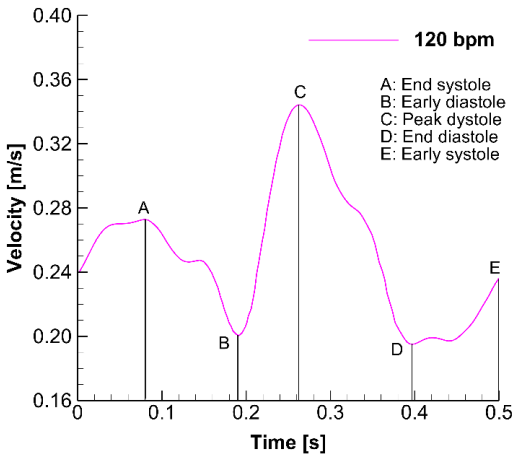

Figure 6. Stages of a heart cycle.

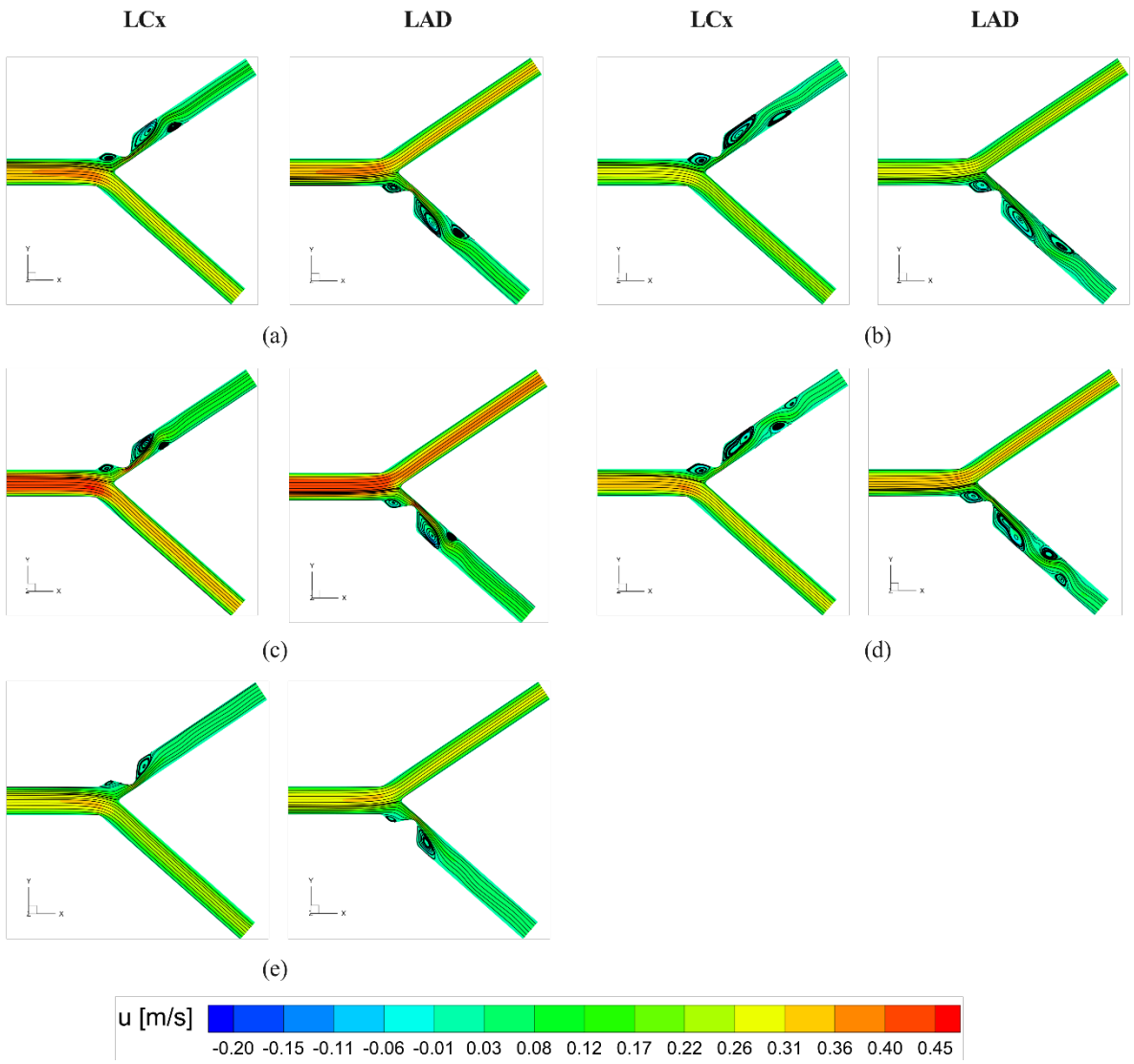

Figure 7. $x-v$elocity streamlines for 75% degree of stenosis at different instants of a cardiac cycle for the LCx and LAD branches: (a) End-systole, (b) Early-diastole, (c) Peak-diastole, (d) End-diastole, (e) Early-systole.

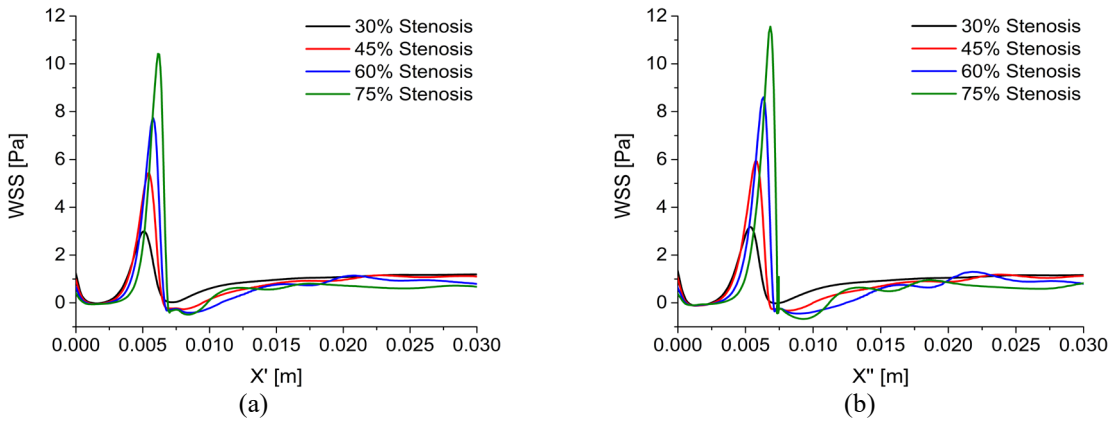

Figure 8**.** Spatial wall shear stress (WSS) variation for different stenosis degrees: (a) LCx, (b) LAD.

Figure 9 displays variations of OSI at the different degrees of stenosis in LCx and LAD. In all the cases, prominent fluctuations of OSI are seen with local peaks near the stenosis centres and circulation zones caused by the vortical structures. The highest value of OSI in LCx and LAD are found to be 0.48 and 0.49 respectively at 45% DOS. For all the other cases, the highest values of OSI in LAD and LCx are equal at corresponding DOS. Further, it is observed that though OSI drops drastically just downstream of the stenosis, it again increases at the distal regions, particularly for 60% and 75% DOS.

Additionally, the rises in OSI values downstream of the stenosis in LAD under such conditions are more than in LCx. This observation is in harmony with the streamline contours presented in Figure 7. Jahromi *et al.* [43] postulated the development of secondary plaque at a region distal to the post-stenosis area for symmetric plaques. The present findings corroborate this theory for asymmetric stenosis as well. Figure 10 shows the pressure variations along LCx and LAD at various degrees of stenosis. The pressure variation follows the same pattern for both branches, where a point of minimum pressure is observed at 60% and 75% DOS, followed by a region of an adverse pressure gradient. Figure 11 plots PD across the stenosis for both vessels under different degrees of stenosis. It is observed that PD across the stenosis is more for LAD compared with LCx at all degrees of stenosis. Further, PD increases with increasing DOS. This is in good agreement with the findings of [16]. It is also noticed that the PD variations between LAD and LCx are higher at severe stenosis, especially at 60% and 75% DOS.

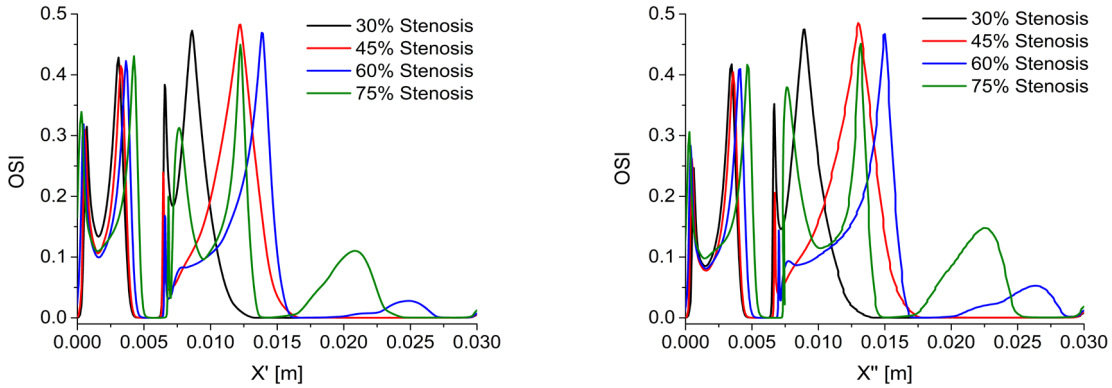

Figure 9**.** Spatial Oscillatory shear index (OSI) variation for different stenosis degrees: (a) LCx, (b) LAD.

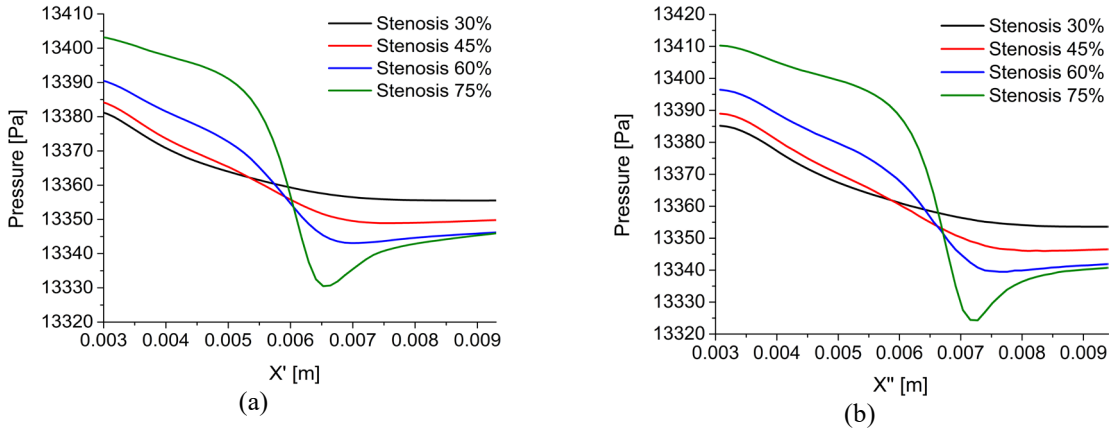

Figure 10. Pressure variation across the plaque for different stenosis degrees: (a) LCx, (b) LAD.

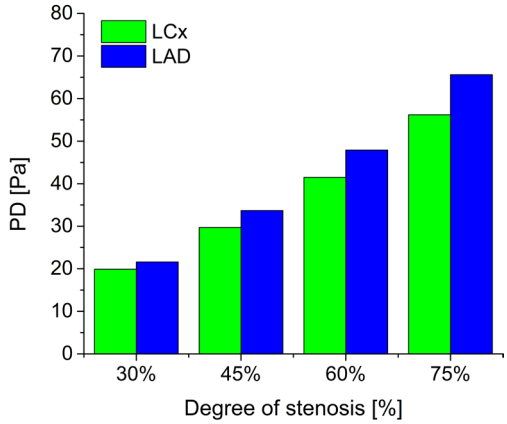

Figure 11. Variation of pressure drop between the beginning and end points of the plaque for different stenosis degrees in the LCx branch and LAD branch.

5. CONCLUSION

In this study, numerical simulation and analysis are carried out for 2D pulsatile flow through the left coronary artery bifurcation with asymmetric stenosis in the left circumflex (LCx) and left anterior descending (LAD) arteries. Different degree of asymmetric stenosis with 30%, 45%, 60%, and 75% are considered for the study. Extensive simulations are carried out to analyse variations of hemodynamic parameters like wall shear stress (WSS), oscillatory shear index (OSI), and pressure drop (PD) across the plaque for different degrees of stenosis at a heart rate of 120 beats per minute (bpm). The study demonstrates the formation of vortex-shedding in the post-stenotic region in both vessels, indicating the possibility of regions with low WSS and high OSI. In LCx, the maximum computed WSS is 10.42 Pa at 75% DOS, whereas the corresponding value in LAD is 11.56 Pa under the same DOS. At all degrees of stenosis, the lowest values of WSS in LAD are lower than the corresponding ones in LCx. The minimum value of WSS registered in the LAD is -0.67 Pa at 75% DOS whereas the minimum value of WSS registered in LCx is -0.49 Pa at same DOS. Even for 30% DOS, the lowest values of WSS in LCx and LAD are found to be -0.02 Pa and -0.12 Pa respectively. indicating that LAD is more prone to faster disease progression in the earlier phase of plaque formation. Although the maximum value of OSI decreases with the increase in the DOS, elevated levels of OSI are found in the distal regions, especially for higher DOS (60% and 75%), indicating susceptibility to the progression of secondary plaque formation. The maximum value of OSI in LAD and LCx are found to be is 0.49 and 0.48 respectively at 45% DOS. The PD increases with increasing in DOS. For a given DOS, the adverse effects are found more severe in the case of LAD than in the case of the LCx. Thus, based on observation we can conclude that a person having a blockage in the LAD branch experiences more cardiovascular risk compared to the same blockages in the LCx branch. The present work bears implications in real clinical applications. However, the scope remains to extend the study to incorporate more complex aspects like three-dimensionality and fluid-structure interactions, which may open up further avenues related to the hemodynamics in stenosed arteries.

ACKNOWLEDGEMENT AND FUNDING

The authors thank the All India Council for Technical Education (AICTE) for providing the AICTE Doctoral Fellowship (ADF) to the corresponding author to carry out the research work.

DECLARATION OF CONFLICTING INTERESTS

The authors declare no potential conflicts of interest with respect to the research and publication of this article.

REFRENCES

[1] World Health Organization, Cardiovascular diseases (CVDs) (website). https://www.who.int/news-room/fact-sheets/detail/cardiovascular-diseases-(cvds), 2021 (accessed 21.03.2023).

[2] I. O. Starodumov, S. Y. Sokolov, D. V. Alexandrov, A. Y. Zubarev, I. S. Bessonov, V. V. Chestukhin and F.A Blyakhman, Modelling of hemodynamics in bifurcation lesions of coronary arteries before and after myocardial revascularization, *Philosophical Transactions of the Royal Society A*, 380(2217), 2022, 20200303.

[3] P. Jhunjhunwala, P. Padole and S. Thombre, CFD analysis of pulsatile flow and non-Newtonian behavior of blood in arteries, *MCB: Molecular & Cellular Biomechanics*, 12(1), 2015, 37-47.

[4] B. Zhang, Y. Jin, X. Wang, T. Zeng and L.Wang. Numerical simulation of transient blood flow through the left coronary artery with varying degrees of bifurcation angles, *Journal of Mechanics in Medicine and Biology*, 17(01), 2017, 1750005.

[5] A. Athani, N. N. N. Ghazali, I. A. Badruddin, S. Kamangar, A. E. Anqi and A. Algahtani, Investigation of two-way fluid-structure interaction of blood flow in a patient-specific left coronary artery, *Bio-Medical Materials and Engineering*, 33(1), 2022, 13-30.

[6] T. Chaichana, Z. Sun and J. Jewkes, Hemodynamic impacts of various types of stenosis inthe left coronary artery bifurcation: A patient-specific analysis, *Physica Medica*, 29(5), 2013, 447-452.

[7] E. Miranda, L. C. Sousa, C. C. António, C. F. Castro and S. I. S. Pinto, Role of the left coronary artery geometry configuration in atherosusceptibility: CFD simulations considering sPTT model for blood, *Computer Methods in Biomechanics and Biomedical Engineering*, 24(13), 2021, 1488-1503.

[8] N. Pinho, C. F Castro, C. C. António, N. Bettencourt, L. C. Sousa and S. I. S. Pinto, Correlation between geometric parameters of the left coronary artery and hemodynamic descriptors of atherosclerosis: FSI and statistical study, *Medical & Biological Engineering & Computing*, 57, 2019, 715-729.

[9] S. I. S. Pinto and J. B. L. M. Campos, Numerical study of wall shear stress-based descriptors in the human left coronary artery, *Computer Methods in Biomechanics and Biomedical Engineering*, 19(13), 2016, 1443-1455.

[10] K. C. Ang and J. N. Mazumdar, Mathematical modelling of three-dimensional flow through an asymmetric arterial stenosis, *Mathematical and Computer Modelling*, 25(1), 1997, 19-29.

[11] J. Frattolin, M. M. Zarandi, C. Pagiatakis, O. F. Bertrand and R. Mongrain, Numerical study of stenotic side branch hemodynamics in true bifurcation lesions, *Computers in Biology and Medicine*, 57, 2015, 130-138.

[12] S. Kamangar, N. J. Salman Ahmed, I. A. Badruddin, N. Al-Rawahi, A. Husain, K. Govindaraju and Y. Khan, Effect of stenosis on hemodynamics in left coronary artery based on patient-specific CT scan, *Bio-Medical Materials and Engineering*, 30(4), 2019, 463-473.

[13] J. Song, S. Kouidri and F.Bakir, Numerical study of hemodynamic and diagnostic parameters affected by stenosis in bifurcated artery, *Computer Methods in Biomechanics and Biomedical Engineering*, 23(12), 2020, 894-905.

[14] F. B. Tian, L. Zhu, P. W. Fok and X.Y. Lu, Simulation of a pulsatile non-Newtonian flow past a stenosed 2D artery with

atherosclerosis, *Computers in Biology and Medicine*, 43(9), 2013, 1098-1113.
[15] T. Sood, S. Roy and M. Pathak, Effect of pulse rate variation on blood flow through axisymmetric and asymmetric stenotic artery models, *Mathematical Biosciences*, 298, 2018, 1-18.
[16] B. Thomas, K.S. Sumam and N. Sajikumar, Patient specific modelling of blood flow in coronary artery, *Journal of Applied Fluid Mechanics*, 14(5), 2021, 1469-1482.
[17] M. Timofeeva, A. Ooi, E. K. Poon and P. Barlis, Numerical simulation of the blood flow through the coronary artery stenosis: Effects of varying eccentricity, *Computers in Biology and Medicine*, 146, 2022, 105672.
[18] M. P. Tulppo, A. M. Kiviniemi, M. Lahtinen, O. Ukkola, T. Toukola, J. Perkiömäki, M. J. Junttila and H. V. Huikuri, Physical activity and the risk for sudden cardiac death in patients with coronary artery disease, *Circulation: Arrhythmia and Electrophysiology*, 13(6), 2020, e007908.
[19] E. Marijon, M. Tafflet, D. S. Celermajer, F. Dumas, M. C. Perier, H. Mustafic, J. F. Toussaint, M. Desnos, M. Rieu, N. Benameur and J. Y. Le Heuzey, Sports-related sudden death in the general population, *Circulation*, 124(6), 2011, 672-681.
[20] F. J. Ha, H. C. Han, P. Sanders, A. La Gerche, A. W. Teh, O. Farouque and H. S. Lim, Sudden cardiac death related to physical exercise in the young: A nationwide cohort study of Australia, *Internal Medicine Journal*, 53(4), 2023, 497-502.
[21] M. Owais, A. Y. Usmani and K. Muralidhar, Effect of a bend on vortex formation and evolution in a three-dimensional stenosed geometry during pulsatile flow, *Physics of Fluids*, 35(3), 2023.
[22] B. Liu and D. Tang, Influence of distal stenosis on blood flow through coronary serial stenoses: A numerical study. *International Journal of Computational Methods*, 16(03), 2019, 1842003.
[23] S. Bahrami and M. Norouzi, A numerical study on hemodynamics in the left coronary bifurcation with normal and hypertension conditions, *Biomechanics and Modeling in Mechanobiology*, 17(6), 2018, 1785-1796.
[24] M. Biglarian, B. Firoozabadi and M. S. Saidi, Atheroprone sites of coronary artery bifurcation: Effect of heart motion on hemodynamics-dependent monocytes deposition. *Computers in Biology and Medicine*, 133, 2021, 104411.
[25] P. J. Blanco, G. H .V. Dos Santos, C. A. Bulant, A. M. Alvarez, F.A. Oliveira, G. Cunha-Lima and P. A. Lemos, Scaling laws and the left main coronary artery bifurcation. A combination of geometric and simulation analyses. *Medical Engineering & Physics*, 99, 2022, 103701.
[26] J. T. Dodge Jr, B. G. Brown, E. L. Bolson and H. T. Dodge, Lumen diameter of normal human coronary arteries: Influence of age, sex, anatomic variation, and left ventricular hypertrophy or dilation, *Circulation*, 86(1), 1992, 232-246.
[27] N. Freidoonimehr, R. Chin, A. Zander and M. Arjomandi, Effect of shape of the stenosis on the hemodynamics of a stenosed coronary artery, *Physics of Fluids*, 33(8), 2021.
[28] Y. Zhou, C. Lee and J. Wang, The computational fluid dynamics analyses on hemodynamic characteristics in stenosed arterial models. *Journal of Healthcare Engineering*, 2018, 4312415.
[29] A. Equbal and P. Kalita, Numerical Analysis to Investigate the Effect of Stenosis Shape on the Hemodynamics of Flow Through a Straight-Cylindrical Artery, *International Conference in Fluid, Thermal and Energy Systems,* 2022, 109-119.
[30] M. K. Christiansen, J. M. Jensen, B. L. Nørgaard, D. Dey, H. E. Bøtker and H. K. Jensen, Coronary plaque burden and adverse plaque characteristics are increased in healthy relatives of patients with early onset coronary artery disease. *Cardiovascular Imaging*, 10(10 Part A), 2017, 1128-1135.
[31] P. Basavaraja, A. Surendran, A. Gupta, L. Saba, J. R. Laird, A. Nicolaides, E. E. Mtui, H. Baradaran, F. Lavra and J. S. Suri, Wall shear stress and oscillatory shear index distribution in carotid artery with varying degree of stenosis: *Journal of Mechanics in Medicine and Biology*, 17(02), 2017, 1750037.
[32] S. Bahrami and M. Norouzi, Hemodynamic impacts of hematocrit level by two-way coupled FSI in the left coronary bifurcation, *Clinical Hemorheology and Microcirculation*, 76(1), 2020, 9-26.
[33] M. Abbasian, M. Shams, Z. Valizadeh, A. Moshfegh, A. Javadzadegan and S. Cheng, Effects of different non-Newtonian models on unsteady blood flow hemodynamics in patient-specific arterial models with in-vivo validation, *Computer Methods and Programs in Biomedicine*, 186, 2020, 105185.
[34] Y. Zhao, H. Wang, W. Chen, W. Sun, X. Yu, C. Sun and G. Hua, Time-resolved simulation of blood flow through left anterior descending coronary artery: effect of varying extent of stenosis on hemodynamics, *BMC Cardiovascular Disorders*, 23(1), 2023, 156.
[35] M. Ferdows, K. E. Hoque, M. Z. I. Bangalee and M. A. Xenos, Wall shear stress indicators influence the regular hemodynamic conditions in coronary main arterial diseases: cardiovascular abnormalities, *Computer Methods in Biomechanics and Biomedical Engineering*, 26(2), 2023, 235-248.
[36] S. Yagi, T. Sasaki, T. Fukuhara, K. Fujii, M. Morita, Y. Suyama, K. Fukuoka, T. Nishino and I. Hisatome, Hemodynamic analysis of a microanastomosis using computational fluid dynamics, *Yonago Acta Medica*, 63(4), 2020, 308-312.
[37] S. Sandeep and S. R. Shine, Effect of stenosis and dilatation on the hemodynamic parameters associated with left coronary artery, *Computer Methods and Programs in Biomedicine*, 204, 2021, 106052.
[38] F. Gijsen, Y. Katagiri, P. Barlis, C. Bourantas, C. Collet, U. Coskun, J. Daemen, J. Dijkstra, E. Edelman, P. Evans and K. Van Der Heiden, Expert recommendations on the assessment of wall shear stress in human coronary arteries: Existing methodologies, technical considerations, and clinical applications, *European Heart Journal*, 40(41), 2019, 3421-3433.
[39] D. N. Ku, D. P. Giddens, C. K. Zarins and S. Glagov, Pulsatile flow and atherosclerosis in the human carotid bifurcation. Positive correlation between plaque location and low and oscillating shear stress, *Arteriosclerosis*, 5(3), 1985, 293-302.
[40] A. Bit, A. Alblawi, H. Chattopadhyay, Q. A. Quais, A. C. Benim, M. Rahimi-Gorji and H.T. Do, Three dimensional numerical analysis of hemodynamic of stenosed artery considering realistic outlet boundary conditions, *Computer Methods and Programs in Biomedicine*, 185, 2020, 105163.

[41] N. Freidoonimehr, R. Chin, A. Zander and M. Arjomandi, An experimental model for pressure drop evaluation in a stenosed coronary artery, *Physics of Fluids*, 32(2), 2020.
[42] X. Chen, J. Zhuang, H. Huang and Y. Wu, Fluid–structure interactions (FSI) based study of low-density lipoproteins (LDL) uptake in the left coronary artery, *Scientific Reports*, 11(1), 2021, 4803.
[43] R. Jahromi, H. A. Pakravan, M. S. Saidi and B. Firoozabadi, Primary stenosis progression versus secondary stenosis formation in the left coronary bifurcation: A mechanical point of view, *Biocybernetics and Biomedical Engineering*, 39(1), 2019, 188-198.